ELSEVIER

International Journal of Heat and Fluid Flow 20 (1999) 455–461

International Journal of HEAT AND FLUID FLOW

www.elsevier.com/locate/ijhff

A numerical study on the mechanism of splashing

Martin Rieber *, Arnold Frohn

ITLR, Institut für Thermodynamik der Luft- und Raumfahrt, Universität Stuttgart, Pfaffenwaldring 31, D-70550 Stuttgart, Germany

Abstract

The impact of a single drop on a liquid film is studied numerically by solving the Navier–Stokes equations for incompressible fluids in three dimensions. The extension dynamics of the splashing lamella is analyzed and compared with theoretical results from the literature. Physically reasonable numerical results for the disintegration of the splashing lamella are obtained by applying disturbances to the liquid film and to the drop. It is shown that for the conditions considered here the Rayleigh instability is a possible driving mechanism for the formation of cusps at the free rim of the splashing lamella. © 1999 Elsevier Science Inc. All rights reserved.

Keywords: Splashing; Rim instability; Finger formation; Volume-of-fluid method

Notation

T	capillary stress tensor
S	cross section area distribution
x, y, z	Cartesian coordinates
D	drop diameter
H	dimensionless film thickness, h/D
k	dimensionless constant in Eq. (6)
T	dimensionless time, tV/D
Δx, Δy, Δz	dimensions of computational domain
R	estimated radius of initial spot
h	film thickness
A	integral of the wall film velocity, Eq. (8)
V	impact velocity
$r_{\mathrm{l,b}}$	lamella radius at $z=h$
$r_{\mathrm{l,r}}$	lamella radius at the free rim
n	number of cusps or fingers
Oh	Ohnesorge number, $\mu_{\mathrm{l}}/(\sigma\rho_{\mathrm{l}}D)^{1/2}$
p	pressure
r_{rim}	radius of the free rim
t	time
f	volume fraction of the liquid
u	velocity vector $\mathbf{u}=(u,v,w)$
V_{rim}	velocity of the rim relative to the sheet
We	Weber number, $\rho_{\mathrm{l}}DV^2/\sigma$
$\overline{u}$	z-averaged wall film velocity

Greek

μ	dynamic viscosity
ρ	density
σ	surface tension coefficient
δ	thickness of the sheet
$\lambda_{\max}$	wavelength with maximum growth rate

Subscripts

g	gas
l	liquid

1. Introduction

The impact of a single drop on a liquid film is a fascinating fluid mechanical phenomenon, which has attracted the attention of scientists since the last century. Famous photographs of impacting drops are due to Edgerton, who used them to demonstrate the capabilities of his stroboscopic flash technique (Edgerton and Killian, 1979). Several quantitative results for splashing drops are available from the literature. Cossali et al. (1997) determined the critical impact energy (critical Weber number) separating the phenomena of deposition and splashing for a wide parameter range. Furthermore, these authors quantified the number of fingers at the free rim of the splashing lamella as well as the size of the secondary droplets emerging from these fingers. A scaling law for the radial extension of the lamella was deduced theoretically by Yarin and Weiss (1995), who present also a rather complete summary of other results for impacting drops. We will countercheck our numerical results and the above-mentioned theory concerning the extension dynamics of the lamella. This will verify our simulations as well as the theory.

The main purpose of this paper is to investigate the instability of the free rim, which leads to the formation of cusps, fingers and secondary droplets. While this instability is well documented photographically by all of the authors cited above, its underlying physical mechanisms are still not well understood. Thus it is up to now not possible to predict the number of cusps on a clear theoretical basis. There exist of course several attempts to explain the rim instability. Cusp formation at the free rim may be explained by considering the rim as a torus subject to the Rayleigh instability. Yarin and Weiss (1995) however conclude that the number of fingers

* Corresponding author. E-mail: martin.rieber@itlr.uni-stuttgart.de

0142-727X/99/$ – see front matter © 1999 Elsevier Science Inc. All rights reserved.
PII: S0142-727X(99)00033-8

observed in experiments is not in agreement with this mechanism. Consequently, they suggested another mechanism based on the fact that a free rim always propagates normally to its local configuration. This behaviour will lead to the formation of cusps, provided that amplitude and wavelength of initial rim perturbations are of comparable magnitude and large compared with the lamella thickness. Recently Gueyffier and Zaleski (1998) suggested a possible mechanism for the formation of fingers in the very early phase of the impact, when surface tension effects are negligible. It will be shown by a detailed analysis of our numerical results that for the impact parameters considered here the mechanism based on the Rayleigh instability can explain the formation of cusps at intermediate times of the splashing process.

The first attempt to simulate the drop impact numerically has been undertaken by Harlow and Shannon (1967). While these simulations can be considered as a milestone of computational fluid dynamics, they are two-dimensional and thus not suited to gain further insight into the mechanism of the rim instability. Fortunately, the capacity of present-day supercomputers makes a three-dimensional simulation of drop impacts with splashing possible. The numerical method used in the present study to simulate splashing drops has been already successfully applied to binary drop collisions (Rieber and Frohn, 1997) and to collisions of drops with hot walls (Karl et al., 1996).

2. Numerical method

The flows considered here are described by the Navier–Stokes equations for incompressible fluids with variable density and viscosity including free interfaces with surface tension

$$\frac{\partial(\rho\mathbf{u})}{\partial t} + \nabla\cdot[(\rho\mathbf{u})\otimes\mathbf{u}] = -\nabla p + \nabla\cdot\mu[\nabla\mathbf{u} + (\nabla\mathbf{u})^{\mathrm{T}}] + \nabla\cdot\mathbf{T}, \tag{1}$$

$$\nabla\cdot\mathbf{u} = 0. \tag{2}$$

The last term in the momentum equation accounts for surface tension according to the conservative model of Lafaurie et al. (1994), where $\mathbf{T}$ is the capillary stress tensor. Density and viscosity are constant inside the gas and the liquid, but vary discontinuously at the sharp interface separating liquid and gas. In the volume-of-fluid method (Hirt and Nichols, 1981) density and viscosity are related to the volume fraction f of the liquid by

$$\rho = \rho_{\mathrm{g}} + (\rho_{\mathrm{l}} - \rho_{\mathrm{g}})f, \tag{3}$$

$$\mu = \mu_{\mathrm{g}} + (\mu_{\mathrm{l}} - \mu_{\mathrm{g}})f. \tag{4}$$

Advection of the liquid volume, and thus of the discontinuity, is governed by the transport equation

$$\frac{\partial f}{\partial t} + \nabla\cdot(\mathbf{u}f) = 0. \tag{5}$$

In the framework of the volume-of-fluid method all flow discontinuities are captured in a straightforward way using conservative finite volume discretizations for Eqs. (1)–(5). Specifically, we use a second-order conservative Godunov projection method on a MAC-grid. A similar method on a collocated grid has been described by Puckett et al. (1997). In contrast to the method mentioned before, the formulation of momentum advection is fully conservative. Conservative momentum advection turned out to be essential for a successful simulation of splashing drops. This is not astonishing because strict conservation ensures that flow discontinuities move with the correct speed (Vinokur, 1989). The computation of volume fluxes is based on a piecewise linear reconstruction of the interface (Puckett et al., 1997). In this way the interface remains sharp even for long time simulations. Like momentum and volume fraction transport, surface tension and momentum diffusion are treated explicitly, while the pressure is determined by an implicit Poisson equation. Discontinuous coefficients in the Poisson equation due to the discontinuous density field cause standard multigrid solvers to fail. It has been found that a cell-centred multigrid method with Galerkin coarse grid approximation is rather insensitive to the density ratio and is also very efficient (Wesseling, 1988). Usually between two and six multigrid V-cycles reduce the velocity divergence sufficiently. A fixed Cartesian grid facilitated the parallelization of the code for parallel supercomputers with distributed memory.

3. Results

The parameters of the splashing process taken into account are film thickness h, diameter D and impact velocity V of the drop, density ρ_{l} and viscosity μ_{l} of the liquid, surface tension σ and time t. A corresponding set of dimensionless parameters is the Weber number $\mathrm{We} = \rho_{\mathrm{l}}DV^2/\sigma$, the Ohnesorge number $\mathrm{Oh} = \mu_{\mathrm{l}}/(\sigma\rho_{\mathrm{l}}D)^{1/2}$, the dimensionless film thickness $H = h/D$ and the dimensionless time $T = tV/D$. Time is zero at the first contact between drop and film. The density and the viscosity ratios are related to a water-air system at normal conditions, thus $\rho_{\mathrm{l}}/\rho_{\mathrm{g}} = 1000$ and $\mu_{\mathrm{l}}/\mu_{\mathrm{g}} = 40$. For these ratios the gas flow has no significant influence on the solution. Physically reasonable numerical results for the disintegration of the splashing lamella are obtained by adding a random disturbance with Gaussian distribution to the initial velocities of film and drop in each control volume. The standard deviation of the disturbance is chosen rather high with up to $0.5V$. Due to viscosity and surface tension the kinetic energy of these disturbances decreases very fast, while being partially transformed into the interfacial energy of small interface disturbances. Without these disturbances, the disintegration of the lamella shows effects which are not observed in experiments. In reality, such disturbances result from flow details in the very early phase after impact, which cannot be resolved within an overall simulation of splashing drops due to their small length and time scales.

Only one quarter of the full problem is simulated using an equidistant Cartesian mesh in a rectangular domain. Plane $z = 0$ is identified with the wall below the film. At the two planes of symmetry with $x = 0$ or $y = 0$ the number of cusps is constrained to exactly one or exactly zero. Thus the number of cusps is always even in our numerical simulations. This constraint should influence the numerical result much less than the inevitable lower grid resolution resulting from a simulation of the full problem. The different combinations of physical and numerical parameters used for the simulations are summarized in Table 1. The Ohnesorge number is given only for completeness; it indicates that viscosity has no significant influence on the solution. The critical Weber number separating splashing and deposition is about 200 for the values of H and Oh considered here, thus all simulations should result in splashing (Cossali et al., 1997).

Table 1
Parameters of splash simulations

Case	We	Oh	H	ΔT	Symmetries	Resolution
A	250	0.0014	0.116	3.5	2	320^3
B	437	0.0016	0.1	3.5	2	256^3
C	598	0.0014	0.116	3.5	2	320^3

Fig. 1 gives an overview of the temporal evolution of the splashing process for three different Weber numbers. The droplet rings at $T=0.6$ result from a torus which has been ejected approximately at $T=0.2$. The splashing lamella is expanding radially, while on its top a rim of increasing diameter is formed. This rim is subject to an instability which forms first cusps, then fingers and finally secondary droplets. In the high Weber number case fingers exist already immediately after impact. It should be noted that the formation of holes between rim and lamella, which is visible for the two simulations at higher Weber numbers, is not observed in experiments. Nevertheless, it will be tried to gain as much insight as possible into the splashing mechanism from the simulations.

Several conclusions may be drawn just from a qualitative inspection of the results in Fig. 1. It is clearly visible that the shape of the intact lamella and its diameter at the bottom depend on time but not on the Weber number, whereas quantities characterizing the shape of the rim on top of the lamella depend on both time and Weber number: For a given time, the diameter of the rim is decreasing with the Weber number, while the number of cusps, of fingers and of secondary droplets increases with Weber number.

The dynamics of lamella and rim are quantified with the help of cross sections at $y=0$ like those in Fig. 2. As a basis for the following analysis, we determine the radial distance $r_{l,b}$ of the bottom of the splashing lamella from these cross sections as a function of time (Fig. 3). Yarin and Weiss (1995) have shown theoretically that $r_{l,b}$ is asymptotically given by

$$\frac{r_{l,b}}{D} = kT^{1/2} \tag{6}$$

with

$$k = \left[\frac{2A}{VD}\right]^{1/2}. \tag{7}$$

The dimensionless constant k depends solely on the velocity distribution of the wall film inside the splashing lamella. More specifically, within the scope of the present paper, A is the integral

$$A = \int_0^{\Delta x} \bar{u}(x)\,\mathrm{d}x \tag{8}$$

of the z-averaged radial velocity in the wall film

$$\bar{u}(x) = \frac{\int_0^h f(x,y=0,z)u(x,y=0,z)\,\mathrm{d}z}{\int_0^h f(x,y=0,z)\,\mathrm{d}z} \tag{9}$$

evaluated at some time not too short after impact.

In order to check not only k, but also the exponent 1/2 in Eq. (6), we fit a power law with two free parameters to the discrete values of Fig. 3. The best fits are

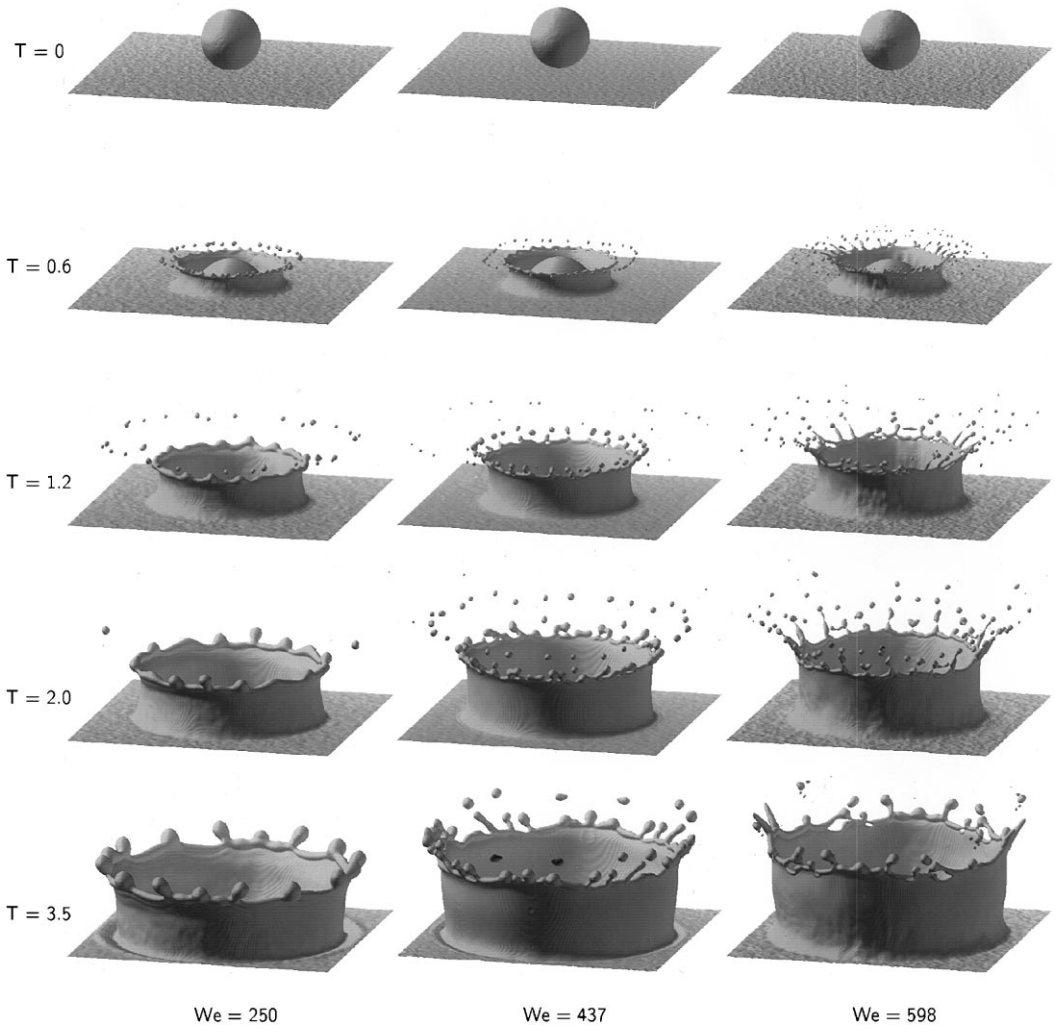

Fig. 1. The shape of the splashing lamella as a function of We and T for cases A, B and C.

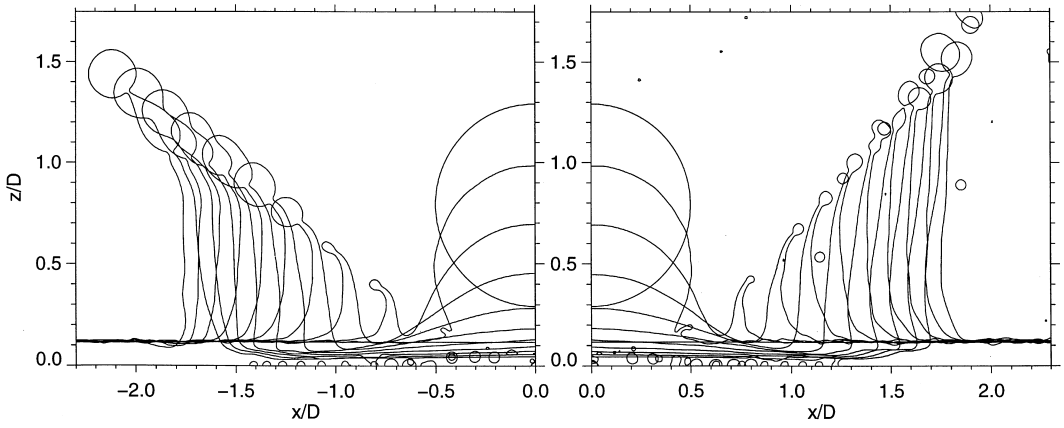

Fig. 2. Vertical cross sections of the splashing lamella for cases A (left) and C (right). The time range for both cases is $0 < T < 3$.

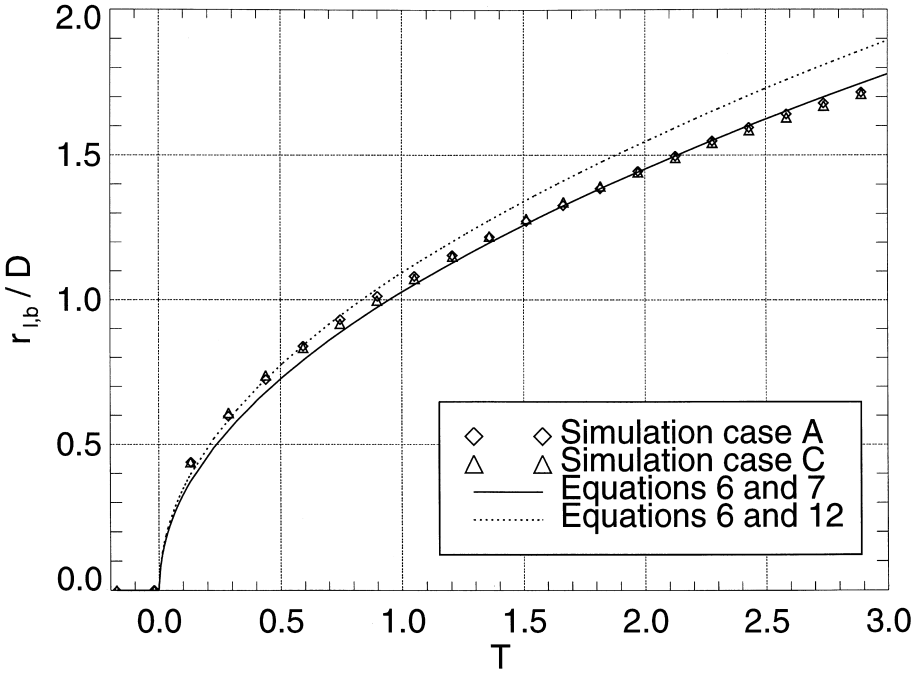

Fig. 3. Radial distance $r_{l,b}$ of the bottom of the splashing lamella as a function of time. Comparison of numerical results for cases A and C with theoretical results of Yarin and Weiss (1995). For reasons of clarity the fitting curves of the numerical data, Eqs. (10) and (11), have been omitted.

case A: $r_{l,b}/D = 1.058T^{0.459}$ (10)

and

case C: $r_{l,b}/D = 1.065T^{0.444}$. (11)

As expected from Fig. 3 and from Eq. (6), the Weber number does not influence the radial extension of the splashing lamella. Furthermore, the best fits essentially confirm the square-root dependency of $r_{l,b}$ on time in Eq. (6). Similar results have been obtained by Gueyffier and Zaleski (1998) for larger values of H.

It is interesting to compare Eqs. (10) and (11) with the asymptotic theory, Eqs. (6) and (7). We evaluate the integral A at $T = 1.2$. At this time A reaches its maximum value, while decreasing slowly for later times. In both cases we arrive at $k = 1.027$, yielding the theoretical time law $r_{l,b}/D = 1.027\ T^{1/2}$. The excellent agreement in Fig. 3 between this theoretical prediction and the observed behaviour is remarkable, the more as strictly speaking the theory applies only to the asymptotic regime $T \gg 1$.

In order to calculate A without detailed knowledge of $\bar{u}$, Yarin and Weiss choose the simple approximation $\bar{u}(x) = V$ for $x < R$, and $\bar{u}(x) = 0$ elsewhere. The radius R of the initial spot produced by the impacting drop is estimated by the volume balance $\pi R^2 h = \pi D^3/6$. This means that the initial spot has the same (average) thickness as the surrounding undisturbed film. The preceding estimates yield $R/D = (6H)^{-1/2}$ and $k = (3H/2)^{-1/4}$.

In our numerical simulations $\bar{u}$ reaches the asymptotic shape of a ramp already at times around $T = 1.2$. At that time

$\bar{u}(x)$ varies linearly between $\bar{u}=0$ at the center of impact and $\bar{u} \approx V$ close to the splashing lamella. Additionally, at that time $r_{l,b}/D$ meets the approximation $R/D=1.2$ from above, as can be seen from Fig. 3. Based on these observations we arrive at the improved approximation

$$k = (6H)^{-1/4}, \tag{12}$$

which yields $r_{l,b}/D = 1.094\ T^{1/2}$ for both cases (see also Fig. 3).

In the remaining, possible driving mechanisms for the rim instability are studied. Forgetting at the moment about more complex mechanisms, the rim is considered as a torus with major radius $r_{l,r}$ and minor radius r_{rim} subject to the Rayleigh instability alone. If the Rayleigh instability has any significance it should be possible to estimate the number of cusps on the rim with the help of the wavelength of the fastest growing disturbance $\lambda_{max} = 9.0147\ r_{rim}$ (Rayleigh, 1878). Because one wavelength corresponds to one cusp, the number of cusps should be simply

$$n = \frac{2\pi}{9.0147}\frac{r_{l,r}}{r_{rim}}. \tag{13}$$

The radius $r_{l,r}$ is determined from Fig. 2. The average value of r_{rim} is determined from the cross section area distribution $S(z) = \int_{\Delta x \Delta y} f(x,y,z)\,dx\,dy$. $S(z)$ shows always a characteristic bump resulting from the free rim. The integral over this bump is the volume of the free rim, from which we obtain r_{rim} using $r_{l,r}$. The best fits of the four data sets (Figs. 4 and 5) based on power laws are given in Table 2 together with the resulting functions for the number of cusps.

For early times after impact, the number of cusps determined from Table 2 and the number of cusps counted in Fig. 1 show only a moderate quantitative agreement (Table 3). Nevertheless, for $T=2.0$ the agreement is excellent. In addition, not only the higher number of cusps for case C is predicted by Eq. (13), but also the slight decrease of the number of cusps with time. Thus the present results indicate that the Rayleigh instability is responsible for the formation of cusps at intermediate times after impact.

In spite of this good agreement, the full rim disintegration mechanism is presumably more complex. In the scenario described above it is assumed that the number of cusps always reflects immediately the actual rim configuration. In reality, however, fingers formed at the cusps will persist over longer times. This might partially explain the discrepancies in Table 3.

Furthermore, the Rayleigh instability does not explain the nonlinear growth of elongated fingers at the cusps. Indeed, finger formation seems to be governed more by the velocity of the free rim relative to the lamella and thus by a mechanism similar to that described by Yarin and Weiss (1995). For a sheet with constant velocity and constant thickness δ the mean velocity of the rim relative to the sheet is (Taylor, 1959)

$$V_{rim} = \left[\frac{2\sigma}{\rho_l \delta}\right]^{1/2}. \tag{14}$$

Note that V_{rim} does not depend on time. While the authors of the present paper were able to reproduce this velocity in their numerical simulations with high accuracy, it was not possible to generate fingers even for initial rim perturbations with large wavelength and amplitude. Thus one may conclude that the varying velocity and/or varying thickness of the actual splashing lamella are responsible for finger formation at the cusps. Especially the velocity varies considerably between bottom and top of the lamella, because as a consequence of Eq. (6) parts of the lamella ejected earlier move much faster than parts ejected at later times. For sheets like the splashing lamella Eq. (14) does no longer hold: V_{rim} is now a function of the actual configuration of rim and lamella. Consequently, the mean velocity of the material collected in the cusps may be different from the mean velocity of the nearby rim. Indeed, in the low Weber number case A of Fig. 1 inertia forces seem to tear the fingers away from the rim.

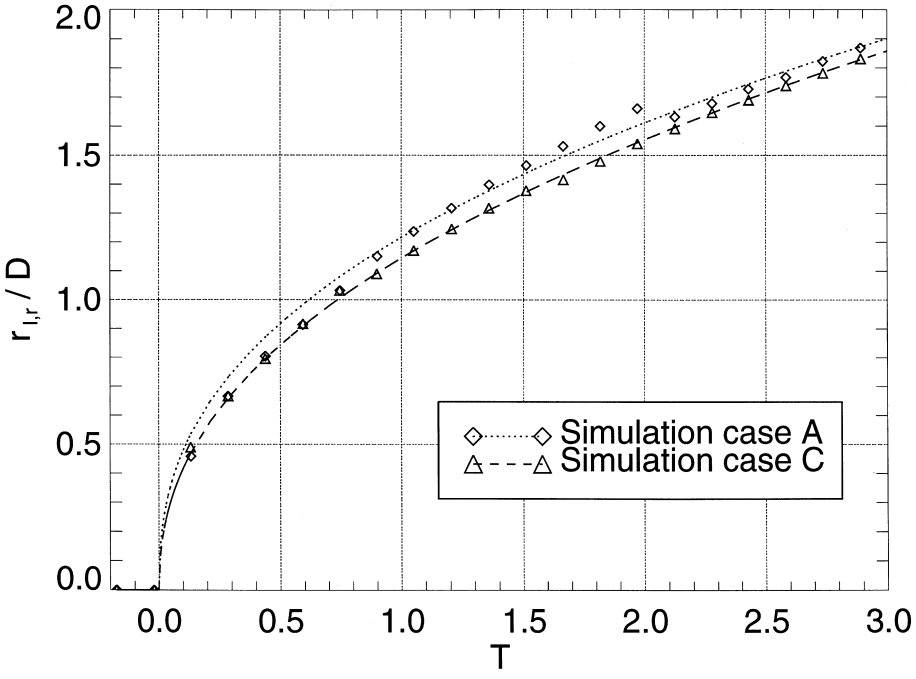

Fig. 4. Radial distance $r_{l,r}$ of the rim on top of the lamella as a function of time for cases A and C.

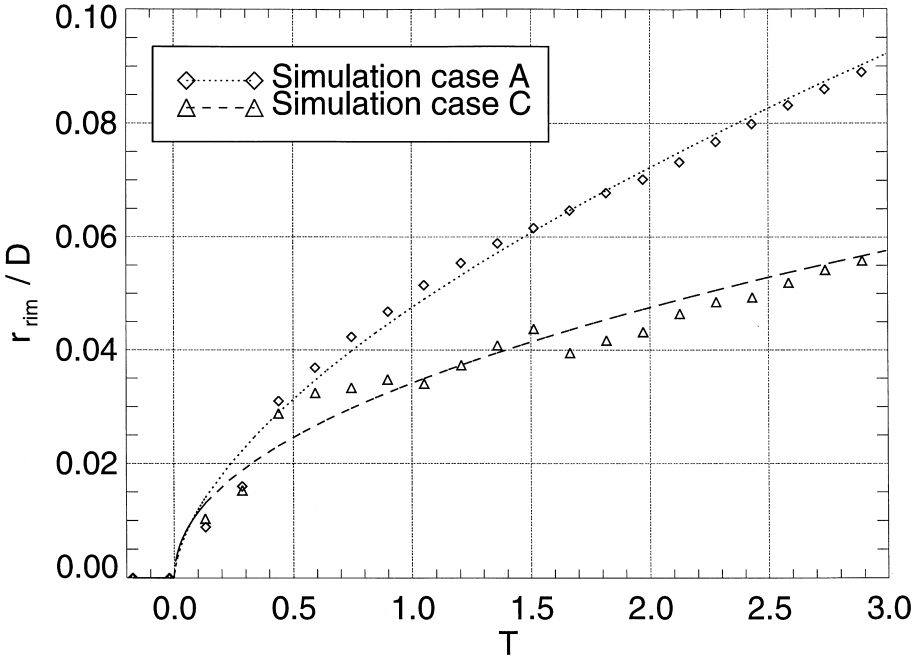

Fig. 5. Radius of the rim on top of the splashing lamella r_{rim} as a function of time for cases A and C.

Table 2
Best fits for $r_{l,r}/D$, r_{rim}/D and resulting functions for the number of cusps n

Case	$r_{l,r}/D$	r_{rim}/D	n
A	$1.22\ T^{0.406}$	$0.0475\ T^{0.604}$	$17.82\ T^{-0.198}$
C	$1.15\ T^{0.441}$	$0.0341\ T^{0.477}$	$23.37\ T^{-0.036}$

Table 3
Comparison between the number of cusps determined from the functions n in Table 2 and the number of cusps counted in Fig. 1

T	0.6	1.2	2.0	3.5
Table 2, case A	20	17	16	14
Fig. 1, case A	22	20	16	16
Table 2, case C	24	23	23	22
Fig. 1, case C	28	24	22	22

4. Conclusion

Physically reasonable numerical results for the disintegration of the splashing lamella have been obtained by disturbing the liquid film and the drop. The extension dynamics of the splashing lamella show a good quantitative agreement with the theoretical results of Yarin and Weiss (1995). It is shown that for the splashes considered here the Rayleigh instability is probably a driving mechanism for cusp formation at the free rim. For later states of the rim instability, the varying thickness and velocity of the splashing lamella might explain the growth of fingers. This assumption should be proved by numerical experiments extracting the basic mechanism.

Acknowledgements

This work was supported by the Deutsche Forschungsgemeinschaft DFG through grant Fr235/43-1. The authors want to thank Dr. Marengo (University of Bergamo, Italy) for his friendly cooperation.

References

Cossali, G.E., Coghe, A., Marengo, M., 1997. The impact of a single drop on a wetted solid surface. Experiments in Fluids 22, 463–472.

Edgerton, H.E., Killian, R.J., 1979. Moments of Vision – The Stroboscopic Revolution in Photography. The MIT Press, Cambridge, Massachusetts.

Gueyffier, D., Zaleski, S., 1998. Formation de digitations lors de l'impact d'une goutte sur un film liquide (finger formation during droplet impact on a liquid film). Comptes Rendus Acad. Sci. Paris sér. II, December 98.

Harlow, F.H., Shannon, J.P., 1967. The splash of a liquid drop. J. Appl. Phys. 38, 3855–3866.

Hirt, C.W., Nichols, B.D., 1981. Volume of fluid (VOF) method for the dynamics of free boundaries. J. Comp. Phys. 39 (1), 201–225.

Karl, A., Anders, K., Rieber, M., Frohn, A., 1996. Deformation of liquid droplets during collisions with hot walls: Experimental and numerical results. Part. Part. Syst. Charact. 13, 186–191.

Lafaurie, B., Nardone, C., Scardovelli, R., Zaleski, S., Zanetti, G., 1994. Modelling merging and fragmentation in multiphase flows with SURFER. J. Comp. Phys. 113, 134–147.

Puckett, E.G., Almgren, A.S., Bell, J.B., Marcus, D.L., Rider, W.J., 1997. A high-order projection method for tracking fluid interfaces in variable density incompressible flows. J. Comp. Phys. 130, 269–282.

Rayleigh, L., 1878. On the instability of jets. Proc. Lond. Math. Soc. 10, 4–13.

Rieber, M., Frohn, A., 1997. Navier–Stokes simulation of droplet collision dynamics. In: Proceedings of the Seventh International Symposium on CFD, Beijing, China, pp. 520–525.

Taylor, G.I., 1959. The dynamics of thin sheets of fluid, iii. disintegration of fluid sheets. Proc. R. Soc. London A 253, 313–321.

Vinokur, M., 1989. An analysis of finite-difference and finite-volume formulations of conservation laws. J. Comp. Phys. 81, 1–52.

Wesseling, P., 1988. Cell-centred multigrid for interface problems. J. Comp. Phys. 79, 85–91.

Yarin, A.L., Weiss, D.A., 1995. Impact of drops on solid surfaces: self-similar capillary waves, and splashing as a new type of kinematic discontinuity. J. Fluid Mech. 283, 141–173.